Modelling of the swelling induced by oxidation in SiC-based refractory castables

Tarek Merzouki, Eric Blond, Nicolas Schmitt, M. Bouchetou, Thierry Cutard, Alain Gasser

▶ **To cite this version:**

Tarek Merzouki, Eric Blond, Nicolas Schmitt, M. Bouchetou, Thierry Cutard, et al.. Modelling of the swelling induced by oxidation in SiC-based refractory castables. Mechanics of Materials, 2014, 68, pp.68 (2014) 253-266. 10.1016/j.mechmat.2013.09.001 . hal-00916918

HAL Id: hal-00916918
https://hal.science/hal-00916918

Submitted on 10 Dec 2013

HAL is a multi-disciplinary open access archive for the deposit and dissemination of scientific research documents, whether they are published or not. The documents may come from teaching and research institutions in France or abroad, or from public or private research centers.

L'archive ouverte pluridisciplinaire **HAL**, est destinée au dépôt et à la diffusion de documents scientifiques de niveau recherche, publiés ou non, émanant des établissements d'enseignement et de recherche français ou étrangers, des laboratoires publics ou privés.

Modelling of the swelling induced by oxidation in SiC-based refractory castables

Tarek Merzouki [a,b], Eric Blond [a], Nicolas Schmitt [c,d], Marie-Laure Bouchetou [e], Thierry Cutard [f], Alain Gasser [a]

[a] *Univ Orléans,PRISME EA4229, 45072 Orléans, France*

[b] *now at LIVS, Univ. of Versailles Saint-Quentin, 78140 Vélisy, France*

[c] *LMT-Cachan, CNRS UMR 8535, ENS Cachan, 94235 Cachan, France*

[d] *Univ. Paris-Est Créteil Val-de-Marne, 93230 Saint-Denis, France*

[e] *CEMHTI UPR3079, Univ. Orléans, 45072 Orléans, France*

[f] *ICA, Mines Albi, 81000 Albi,France*

Abstract

Silicon Carbide-based Refractory Castables (SiC-RC) have high mechanical and chemical resistances at high temperature. Nevertheless when subjected to both high temperature and aggressive oxidizing environment, due to phase transformation, a chemical strain appears that leads to additional stresses in industrial parts and may cause degradation. In this paper, macroscopic constitutive equations are proposed to model the complex relationship between stress, strain, temperature and oxidizing atmosphere in porous SiC-RC. To model the kinetics of the chemical swelling, oxygen content in the porosity of the heterogeneous material is estimated. It depends on both the oxidation reaction of SiC-based grains and the diffusion of oxygen through the connected porosity in the castable. The macroscopic chemical strain associated

to the local SiO_2 formation takes only place when the local small voids are enough filled by the reaction product. Beside, the reduction of porosity is accompanied by a reduction in the gas permeability and consequently a reduction in the diffusion of oxygen.

The multi-physical model is implemented in the finite element code Abaqus®. It accounts for heat transfer, reactive oxygen transport and chemical induced strain. A validation test was carried out on a cylindrical sample subjected to high temperature with a thermal gradient in ambient air. Comparison between experimental results, microscopic observations and numerical results showed that the model provides a good description of the main physical phenomena.

Key words: SiC-based castables; Ceramics; Thermo-chemo-mechanical model; SiC oxidation; Chemical induced strain

1 Introduction

In high temperature industrial plants, refractories are widely used as shields to protect operating equipments against high temperature and aggressive working environment [1]. The inner side of the shields is in contact with complex chemical components at high temperature like slags, fumes, ashes, ..., whereas the opposite side is in contact with a colder part e.g., a tube wall, a safety lining or a timbering.

It is well accepted that the degradation of linings results from complex in-

Email address: eric.blond@univ-orleans.fr

Tel. : +33 (0)2 38 49 43 58

Fax. : +33 (0)2 38 41 73 73 29 (Eric Blond).

teractions between thermal solicitations, mechanical load and constraint and phase transformations induced by chemical reactions [2]. Numerous studies based on physico-chemical analyses are reported in the literature. They are helpful to understand the complex degradation and to improve the resistance and lifetime of such parts. However there is an increasingly need to have recourse to a complete multi-physical analysis coupling experiments and numerical simulations to better describe the degradation mechanisms and their interactions [3,4].

Silicon-carbide based refractory castables (SiC-RC) are prime candidates for many industrial applications involving severe conditions. Compared to other oxide refractories, they exhibit outstanding castables mechanical properties: high strength, high thermal shock resistance, high abrasion-resistance. Their high thermal conductivity makes easier the heat transfer when the shield is a part of a heat exchanger. SiC-RC also have a good resistance to corrosion and oxidation [5,6,7]. However when they are used as protective lining in waste-to-energy plants, based on SEM observations of worn oxide bonded SiC-based refractory tiles, Prigent et co-workers have shown that they progressively corrode with production of new phases mainly in the matrix binder and in the porosity [7,8].

Corrosion of SiC-RC in contact with severe chemical environments involves complex mechanisms with several multiple chemical reactions depending on the nature of chemical species in fluid, on the temperature and on the transport properties across the lining [9]. It does not necessary lead to a deterioration of the mechanical properties of the SiC-based refractory but can induce a swelling which is responsible of additional stresses and may lead to failure of tiles. In that case, having a model describing the stress-strain relationship

-including this chemical swelling at a macroscopic scale and taking finite element simulations- should be useful to improve the design of protective shield and consequently the lifetime of the lining.

Oxidation of SiC-based refractory linings is a common phenomenon observed in high temperature applications. It occurs both at the surface and in the bulk because of the high open porosity typically ranging between 12 and 17 %. A silicon oxide SiO_2 layer forms, covering the surface of the silicon carbide grain and growing under certain conditions. An expansion of the composite grain results, the final volume to the initial volume ratio of small sized grains -mainly located in the binder phase- being more important than those of larger sized grains. At microscopic scale this swelling is first stress-free causing a reduction in the porosity by clogging the pores with no observable macroscopic deformation [8]. When the pores are locally clogged, the increase of the silicon oxide layer in contact with the walls of neighboured grains press them, leading to a macroscopic deformation. As a consequence, a macroscopic volumetric strain of the material occurs and the oxygen diffusion rate decreases with the filling of the pores [10].

In this work, attention is focused on the modelling of one corrosion mechanism in SiC-RC, namely the local passive oxidation of SiC particles. This choice is justified by the fact that this reaction is present in many high temperature applications. The proposed model includes several phenomena, notably transport of oxygen by diffusion in the gas mixture, through the porosity and the induced overall chemical swelling.

The first part of the paper describes the material and experiments and reminds the main dry oxidation mechanisms. The experimental characterisation

of the oxidation behaviour of the SiC-RC is based on isothermal thermogravimetric analysis (TGA) and dilatometric analysis (DA). It is completed with an original experimental test of oxidation performed on a cylindrical sample subjected to a thermal gradient during two months. Experimental results are enriched with scanning electron microscope (SEM) observations and energy-dispersive X-ray spectroscopy (EDS) analyses. The second part details the governing equations of the multi-physics model, the simplifications made and the identification of some parameters. The implementation methodology of the model in a finite element code is shortly described in the third part as well as the model for the numerical simulation of the oxidation test under a thermal gradient. Some results are shown. The last section discusses the results from the model in regard to experimental measurements and observations.

2 Experimental procedures

2.1 Material characteristics

The material of this study is a commercial refractory castable composed of SiC-aggregates, having a particle size distribution ranging from 20 μm to 3 mm and a calcium aluminate based cement [11]. A typical micrography of the microstructure is shown in Fig. 1.a. SiC-RC contains approximately 85 wt% of SiC-grains. The fraction of castable containing the calcium aluminate phase and SiC-particles with size smaller than 200 μm is considered arbitrarily as the matrix phase surrounding the larger SiC-aggregates (Fig. 1.b). Its porosity is equal to 17 % in volume. Some large pores are observed at the millimetre scale but the connected porosity (small pores, microcracks) mainly

exists at the micrometre scale, so that most of the oxidation effects take place in the matrix phase.

SiC oxidation has been extensively studied in various oxidizing environments [5,6,12,13,14,15,16,17]. Two oxidation mechanisms exist depending on the environment and temperature, viz passive and active oxidations.

Passive oxidation of SiC is observed at high temperatures and for partial pressure of oxygen P_{O_2} higher than a critical value $P_{O_2}^{max}$. In absence of water vapour the passive oxidation of SiC is governed by the global reaction

$$SiC(s) + \frac{3}{2}O_2(g) \Longleftrightarrow SiO_2(s) + CO(g) \tag{1}$$

This oxidation mechanism is characterized by the formation of a dense amorphous silica layer SiO_2 surrounding the SiC-grains and of carbon monoxide CO gas escaping in the environment [18]. It leads to a solid mass increase which either improves or deteriorates the mechanical properties of the material depending on the environmental conditions. The oxidation kinetics is controlled by the local diffusion of dioxygen O_2 and carbon monoxide CO through the layer around the SiC-grain which limits oxidation to low extent rates [19]. The isothermal kinetics is generally characterized by a parabolic rate model over a wide temperature range [20].

The dry active oxidation of SiC is governed by the global reaction

$$SiC(s) + O_2(g) \Longleftrightarrow SiO(g) + CO(g) \tag{2}$$

This oxidation mechanism occurring for partial pressure of oxygen, P_{O_2}, lower than a critical value, $P_{O_2}^{min}$, is characterized by the formation of gas phases escaping in the environment [18]. It leads to a solid mass loss which has a

detrimental effect on the mechanical properties.

The active-to-passive oxidation transition was also widely studied in the past [20,21,22] because it is a critical factor influencing the nature of the microstructure and the mechanical properties of SiC after oxidation.

2.2 Isothermal oxidation behaviour

Bahloul characterised the isothermal oxidation of SiC-RC by isothermal thermogravimetric analysis (TGA) under an air flow of 4 ml$\times$min^{-1} on 1g-specimen [23]. Tests were performed at 1000 ^{o}C and 1200 ^{o}C for 50 hours and showed a mass increase (Fig. 2a). Both curves follow a classical square root increase of time curve, which is typical of passive oxidation. As expected for the same duration, the mass gain is higher at higher temperature.

Oxidation of SiC-RC is accompanied by a swelling of the material. In order to evaluate this expansion, Bahloul [23] performed also Isothermal Dilatometry Tests (IDT) on prismatic specimens 9 mm$\times$9 mm$\times$15 mm at 1000 ^{o}C and 1200 ^{o}C. The expansion versus time curves are shown in Fig. 2b. As already observed for the mass gain, the induced expansion is larger for higher temperatures.

More details concerning the experimental device and methodology concerning the isothermal TGA and IDT on this refractory are also available in Doncieux et *al* [11].

2.3 Oxidation under quasi-permanent thermal gradient

To validate the model proposed in this paper, a specific test was performed to oxidise a specimen subjected to a quasi-permanent high temperature gradient (Fig. 3). This test was also designed to be able to reproduce the thermal gradient that such refractory castables have to withstand for long term in service. So, the specimen was previously chemically stabilized for five hours at 800 ^{o}C to complete the dehydration and sintering processes, in accordance with supplier recommendation.

The sample was a cylinder 35 mm in diameter and 150 mm in length. Its upper part was placed in a furnace. The top surface, denoted the hot face was in contact with the air present in the chamber. The furnace was heated, then maintained at a temperature of 1150 ^{o}C. The bottom surface was set on a dense colder vitreous silica support. The lateral surface of the cylinder was covered with a 4 mm thick fibrous insulator, except the upper area. This arrangement permitted to subject the cylinder to a controlled thermal gradient of about 500 ^{o}C,so that the temperatures in the sample were in the range 1150 ^{o}C to 650 ^{o}C. The sample was equipped with four embedded thermocouples (type K) located on the cylinder axis. The stationary temperature field was reached after few hours while the test lasted 56 days.

The diameter of the lasted cylinder was measured at room temperature in two perpendicular directions (D_1 and D_2) all along the sample length with a step of one millimetre with a calliper having an accuracy of 0.01 mm. The measurement was made after the stabilization heat treatment at 800 ^{o}C and after the sample had spent 1350 hours in the device with the furnace at 1150 ^{o}C.

The measurements of the diameter before and after the test, and the resulting variation, are plotted on Fig. 4. The diameters did not exhibit measurable change at distances greater than 75 mm from the hot face. In the forty first millimetres from the hot face, a significant swelling was observed.The maximum being reached at the hot face.

After oxidizing the sample was cut and polished sections were observed by SEM with backscattered electrons (BSEM) (Fig. 5). In contact with SiC-particles at high temperature, O_2 reacted with SiC and a layer of SiO_2 was produced. Small size SiC grains in the matrix seemed more reactive than coarse grains because their higher specific surface. The formation of this layer at the SiC-particle surface led to a reduction in the matrix porosity, and consequently to its densification. The thickness of observed SiO_2 layer is larger close to the hot face and decreases when the distance from the hot face increases. For a distance from the hot face greater than 40 mm, no silica layer was observed.

3 Governing equations

Developing a model describing the macroscopic thermomechanical behaviour of SiC-RC and the effect of the SiC-grains oxidation requires accounting for the physical phenomena implied, viz. thermo-mechanical behaviour, heat conduction, diffusion of gas species, chemical reaction of oxidation and their interactions. Such models, dedicated to porous media , which avoid a detailed description of the microstructure behaviour have already been developed in other domains, notably in civil engineering, for concrete, a material having similar microstructure to those of SiC-RC (grains embedded with a matrix

phase). Some models permit to predict leaching of concrete [24,25,26], crack development linked to alkali-silica reaction [27], hygro-thermal behaviour at high temperatures [28] or deformation and stress in porous solids from in-pore drying-induced crystallization of salt [29].

In most applications, except for those concerning the prediction of the fire behaviour of concrete, the temperature in the parts is low(typically lower than 40 ^{o}C) and almost constant. Also homogeneous behaviour can be assumed and phase transformations are characterised by a low kinetic rate. Conversely, refractory linings are subjected to non-uniform temperatures with value higher than 600 ^{o}C and up to 1700 ^{o}C in some applications. There is a great difficulty to access to quantitative data of material at high temperature . Moreover the strong influence of the temperature distribution and range makes difficult the understanding and the identification of the thermo-chemo-mechanical interactions observed in worn parts or structures.

The macroscopic thermo-chemo-mechanical model is build in the classical framework of thermodynamics of irreversible processes (TIP) applied to open continuous reactive media [30]. The balance equations (mass, momentum, energy) and the constitutive equations (state laws and evolution laws), are the bedrocks of this framework permitting to ensure consistency of the model.

Herein the equations are written at a local macroscopic scale. This means that a Representative Volume Element (RVE) of the SiC-RC exists and that macroscopic variables can be defined at the RVE scale. Also the macroscopic balance and constitutive equations can be linked to the microscopic ones by averaging techniques. Consequently the RVE must be large enough so that a macroscopic behaviour is independent of the material point selected in the

structure [30]. Such macroscopic approach does not permit a high accuracy description of all physical phenomena observed at the microstructure scale but it makes possible to build a numerical tool that is well adapted for the design of the refractory linings using finite element computations. Due to the high connected porosity the RVE is an open porous medium exchanging gas and in particular oxygen with its surrounding. It is undergoing uniform solicitations and embedded in a larger system that is undergoing not uniform loads.

3.1 Balance equations

In service, a mixture of gas (air or aggressive atmosphere) flows through the porosity of SiC-RC. Some species of the gas are inert, some species react with the solid particles and partly disappear and other species are produced by the chemical reactions for example by oxidation (See Eqs. 1-2).

It is underlined that the mixture change of gas does not change the porosity and that each gaseous species occupies the same porous space of the RVE. That is not the case for the solid skeleton. When chemical reactions take place, reactive solid species partly disappear so that the removed volume content converts into porosity and vice-versa solid matter can depose on the skeleton leading to a reduction in the porosity.

The mass balance for each species i contained in the unit volume of RVE in presence of N_r chemical reactions reads [31]

$$\rho \dot{x_i} = -\mathrm{div} J_i + \sum_{r=1}^{N_r} \nu_{ir} M_i \dot{\xi_r} \tag{3}$$

Eq. 3 expresses that the mass content variation of species i in the unit volume

of the RVE is due to partly an external gas flow (first term on the right side) and partly chemical reactions (second term on the right side). The effective bulk density of the RVE is given by $\rho = (1-\phi)\rho_s + \phi\rho_g$, where ρ_s is the mesoscopic or intrinsic mass density of the solid skeleton, ρ_g is the mesoscopic or intrinsic mass density of the gas mixture and ϕ the porosity. Variable x_i is denoted the mass title of species i contained in a unit volume of RVE, i.e. the mass of species i divided by the total mass of the RVE, $(\cdot)$ denoting the time derivative. J_i is the (external) mass flux vector of species i, ν_{ir} is the stoichiometric coefficient of species number i in the r^{th} chemical reaction ($\nu_{ir} < 0$ for the reactants, and $\nu_{ir} > 0$ for the products). M_i is the molar mass of species i. $\dot{\xi}_r$ is the rate of extent of the reaction r, i.e. the rate of formation of molecules of species i divided by stoichiometric coefficient ν_{ir} for the reaction r^{th}.

The set of balance equations (Eq. 3) applies in the general case of oxidation of SiC to account for the influence of the partial pressure of oxygen, or when the global reaction summarizes several elementary reactions, notably in the presence of vapor.

The momentum balance is applied to the porous material to describe the motion of the different constituents, i.e. solid skeleton (s) and gas mixture (g), in the RVE. It reads

$$\operatorname{div}(\boldsymbol{\sigma}^s) + (1-\phi)\rho_s\left(f_s - \boldsymbol{\gamma}_s\right) - f_{int} = 0 \tag{4}$$

and

$$\operatorname{div}(\boldsymbol{\sigma}^g + \phi\rho_g\left(f_g - \boldsymbol{\gamma}_g\right) + f_{int} = 0 \tag{5}$$

where $\boldsymbol{\sigma}^j$ are the partial Cauchy stress tensors in the RVE for the phases $j = s, g$, f_j are body force vectors, $\boldsymbol{\gamma}_j$ is the time derivative of the velocity v_j

vector and f_{int} the body interaction force vector between the two phases.

It should be mentioned, however, that :

- the partial stress tensor $\boldsymbol{\sigma}^j$ is related to the average stress tensor $\overline{\boldsymbol{\sigma}}_j$ prevailing in phase j, i.e., $\boldsymbol{\sigma}^s = (1-\phi)\overline{\boldsymbol{\sigma}}_s$ and $\boldsymbol{\sigma}^g = \phi\overline{\boldsymbol{\sigma}}_g$ respectively;
- Eq. 5 written for the gas mixture applies also for each separated gas phase contained in the mixture.

The overall Cauchy stress tensor $\boldsymbol{\sigma}$ in the RVE is decomposed as

$$\boldsymbol{\sigma} = \boldsymbol{\sigma}^s + \boldsymbol{\sigma}^g \tag{6}$$

The energy balance equation for the reactive porous material is expressed as

$$\dot{e} + \operatorname{div}(q_g) - \boldsymbol{\sigma} : \dot{\boldsymbol{\epsilon}} + \operatorname{div}(q_{th}) - r = 0 \tag{7}$$

where e is the volume density of the internal energy of the whole RVE, q_g is the enthalpy flux transported by the N_g gas species, q_{th} the heat flux, r is the local volume density of the external heat source.

The second law of thermodynamics expressing the non-negativeless of the internal production of entropy reads [30]

$$\dot{s} + \sum_{j=1}^{j=N_g} \operatorname{div}(s_j J_j) + \operatorname{div}\left(\frac{q_{th}}{T}\right) - \frac{r}{T} \geq 0 \tag{8}$$

where s is the volume density of the entropy of the whole RVE, s_j the mass density of the entropy of the gaseous species j.

3.2 Constitutive equations

The set of constitutive equations of the problem are composed of state laws (defined for each phase) and evolution laws, including heat conduction, chemical diffusion, oxidation kinetics, etc. Below the main equations are detailled.

3.2.1 Diffusion of gaseous species

The gas species are transported by diffusion within the air in the porosity of the refractory. The mass flux of species i can therefore be defined using Fick's law [30]

$$J_i = -D_i \,\mathrm{grad}\,(\rho x_i) \tag{9}$$

where D_i is the effective diffusion coefficient of species i in the RVE. The gaseous diffusion into the porosity is hindered by the sizes of pores/microcracks and by the tortuous nature of the network. Taking into account the porous topology effects the effective diffusivity coefficient D_i is linked to the diffusion coefficient D_{0i} existing in the free space filled with the same mixture than those in the porosity

$$D_i = D_{0i} \times f(\phi, \delta, \tau) \tag{10}$$

In Eq. 10, $\tau > 1$ and $\delta < 1$ are dimensionless factors according for tortuosity and constrictivity of the voids, respectively, and ϕ is the actual porosity of the RVE. D_{0i} is given by the Chapman-Enskog equation which is derived from the kinetic theory of gases [32,33]. In the literature, several models have been developed to express the relationship between D_i and D_{0i} [34,35,36]. In this study, due to a lack of available data, the effective diffusivity only depends on

the porosity and is reduced to

$$D_i = D_{0i}\frac{\phi}{\phi_0} \tag{11}$$

Thanks Eq. 11 the effect of the porosity clogg-up during oxidation can be taken into account. Notice that a more complex and realistic relationship can be used if data are available for its identification.

3.2.2 Porosity evolution

The volume fraction ϕ_{ij} -per unit volume of the RVE- occupied by the solid species i occuring or disappearing during the j^{th} chemical reaction is expressed as

$$\phi_{ij} = V_i \nu_{ij} \xi_j \tag{12}$$

where V_i is the molar volume of the solid species i. When ϕ_{0i} is the initial volume fraction of the RVE occupied by the solid species i -i.e. before any chemical reaction-, the volume fraction of the RVE occupied by species i reads

$$\phi_i = \phi_{0i} + \sum_{j}^{N_r} \phi_{ij} \tag{13}$$

Then, The relation between porosity and chemical extents can then be established and reads

$$\phi = \phi_0 + \sum_i (\phi_{0i} + \sum_j V_i \nu_{ij} \xi_j) \tag{14}$$

where ϕ_0 is the initial porosity of the porous media.

3.3 Heat transfer

As shown in Eq. 7, mainly four phenomena supplies on energy transfer namely the classical thermal diffusion (q_{th}), the external volume density heat source

(r), mechanical energy supply and the energy transported by the mass of the gas flowing through the RVE (q_g). As usual, heat conduction in the isotropic RVE is described by the Fourier's law

$$q_{th} = -\lambda grad(T) \tag{15}$$

where λ is the coefficient of effective thermal conductivity of the whole porous medium. In practice, λ depends on several microstructural parameters, in particular the composition of the solid and gaseous phases and the porosity.

The energy flux due to the transport of gaseous species reads

$$q_g = \sum_{j=1}^{N_g} \left(e_j + \left(\frac{p}{\rho_j} \right)_j \right) J_j \tag{16}$$

where e_j is volume density of the internal energy of the gas species j and p is the total gas pressure in the porosity. This contribution as well as those of the heat source r and the mechanical energy supply $\boldsymbol{\sigma} : \dot{\boldsymbol{\epsilon}}$ are low in comparison to the classical term of heat diffusion.

3.4 Kinetics of dry passive oxidation of SiC

Following the macroscopic approach, the oxidation kinetics is described at the RVE scale with a macroscopic model. The kinetic law is developed considering thermodynamics of irreversible processes close to the equilibrium. From a general point of view, assuming a first order reaction after reaching the activation temperature, the extent rate $\dot{\xi}$ is defined by [37,38]

$$\dot{\xi} = k \prod_{j,\ \nu_{ji}<0} c_j \left(1 - \frac{Q}{k^{eq}} \right) \tag{17}$$

where k is is the kinetic factor of the reaction and c_j is molar concentration of the specie j. k^{eq} and Q are the equilibrium constant and the mass action law product of the reaction respectively. When chemical equilibrium is reached, the extent rate is equal to zero and the mass action product Q is equal to the equilibrium constant k^{eq}.

This work focuses on passive oxidation for long term prediction of SiC oxidation. Furthermore, the crystallization of the formed silica layer which modifies the oxidation kinetics and is expected to occur after a long reaction time at higher temperature [39] is not considered. Thus, at each material point, to account for the local passive oxidation inside the RVE, Eq. 17 is written considering a parabolic rate law

$$\dot{\xi} = \frac{1}{2}\frac{k_p}{\xi}\left(\frac{\rho x_{O_2}}{M_{O_2}}\right)^2\left(1-\frac{Q}{k^{eq}}\right)^2 \tag{18}$$

where the kinetics factor k_p follows Arrhenius law

$$k_p = k_p^0 e^{\left(-\frac{E_p}{RT}\right)} \tag{19}$$

k_p^0 being a pre-exponential constant and E_p the activation energy of the passive oxidation.

3.5 Strain behaviour

In the range of temperature concerned in waste-to-energy plant applications, at the RVE scale, SiC-RC materials exhibit an isotropic thermo-elastic quasi brittle behaviour with small strains. The effective total strain tensor $\boldsymbol{\varepsilon}$ in the RVE can be decomposed into three parts, namely an elastic strain tensor, $\boldsymbol{\varepsilon}^e$, a thermal strain tensor, $\boldsymbol{\varepsilon}^{th}$, and a chemical strain tensor, $\boldsymbol{\varepsilon}^{ch}$, induced by the

oxidation

$$\boldsymbol{\varepsilon} = \boldsymbol{\varepsilon}^e + \boldsymbol{\varepsilon}^{th} + \boldsymbol{\varepsilon}^{ch} \tag{20}$$

The elastic strain tensor $\boldsymbol{\varepsilon}^e$ is related to the effective stress tensor $\boldsymbol{\sigma}$ through the elasticity law

$$\boldsymbol{\varepsilon}^e = \frac{1+\nu}{E}\boldsymbol{\sigma} - \frac{\nu}{E}Tr(\boldsymbol{\sigma})I \tag{21}$$

where I is the second rank unit tensor, E and ν are the Young's modulus and the Poisson's ratio of the solid skeleton, respectively. These parameters are not necessary constant and depend on the phases content and properties as well as the porosity. The thermal strain tensor is related to the isotropic coefficient of thermal expansion, α, and to temperature, T

$$\boldsymbol{\varepsilon}^{th} = \alpha(T - T_{ref})I \tag{22}$$

where T_{ref} is the reference temperature.

Experiments have confirmed that the strain induced by oxidation of SiC linearly depends to the chemical extent ξ. Consequently, the isotropic second rank tensor describing the chemical strain tensor, $\boldsymbol{\varepsilon}^{ch}$, is expressed as

$$\boldsymbol{\varepsilon}^{ch} = \beta \left\langle \xi - \xi_{cr} \right\rangle I \tag{23}$$

where β is the coefficient of effective chemical expansion, ξ_{cr} is the critical extent of oxidation and $< . >$ denotes the positive part of the content in the brackets.

3.6 Reduced model

It is difficult to identify the complete model described previously for the study of the corrosion by SiC oxidation in protective linings tiles used in waste-to-

energy plants. Indeed there exist a great variability of the material and the complex history of in situ conditions of the aggressive environment (ashes and fumes) are not well known. Thus a reduced or simplified model is derived from the previous model. The simplifications are detailled below.

3.6.1 Mass balance

The mass balance (Eq. 3) is only written for the diffusion and consumption of dioxygen contained in the fumes. Indeed very low gas flux exists at the cold face of lining tiles which is in contact with a metallic part. Moreover, the source term in (Eq. 3) is limited to the description of the kinetics of dry passive SiC oxidation (Eq. 1). Indeed this chemical reaction is the first occurring before other chemical reactions between silica and ashes and fumes take place. As it was observed on worn tiles and the sample oxidised under temperature gradient the localization of the induced expansion is not modify by the complete corrosion process. Consequently the strain field is reasonably predict with a model accounting only for SiC oxidation.

To simplify the implementation of the model in the Finite Element (FE), the partial pressure of oxygen, P_{O_2}, is chosen as state variable instead of the mass title of oxygen x_{O_2} in the RVE.

The mass balance (Eq 3) is then rewritten assuming ideal gas behaviour

$$\frac{\partial P_{O_2}}{\partial t} = \operatorname{div}\left(D_{O_2} \operatorname{grad}\left(P_{O_2}\right)\right) + RT\nu_{O_2}\dot{\xi} \tag{24}$$

where the oxygen stoichiometric coefficient ν_{O_2} is equal to -3/2 and the effective diffusivity of oxygen D_{O_2} only depending on the porosity is given by Eq. 11.

3.6.2 Energy balance and heat transfer

Some simplifications are also made in Eq. 7 in regard to the target industrial applications:

- In Eq. 7, the terms $\mathrm{div}\,(q_g)$, $\boldsymbol{\sigma} : \dot{\boldsymbol{\epsilon}}$ and r are neglected in comparison to the thermal flux $\mathrm{div}\,(q_{th})$ because the passive oxidation is a slow phenomenon, mechanical energy supply is very low and the mass flow of gas species too;
- the gain in mass remains also mild so that the mass density of the RVE is assumed constant and the specific internal energy $e \approx \rho_s \mathcal{C}_p T$;
- the effective coefficient of thermal conductivity λ is assumed constant and equal to the initial value because the SiC mass content remains high even after oxidation. This means also that the influence of the porosity is not taken into account.

These simplifications permit to separate completely the thermal problem from the other physical problems.

3.6.3 Momentum balance simplifications

The gas pressure in the pores of the SiC-RC is negligible compared to the thermomechanical stresses occurring in the solid phase. Consequently, it is assumed that the overall stress tensor $\boldsymbol{\sigma}$ in the porous media is egal to the partial stress tensor in the solid skeleton, i.e., the effective stress, $\boldsymbol{\sigma}^s$ (Eq. 6). Moreover, as the gas flow is slow is not taken into account and its mass balance is neglected. Then,neglecting also the gravity and the dynamic effect, the general momentum balance equations (Eqs. 4-5) reduce to the equation

$$\mathrm{div}\boldsymbol{\sigma} = 0 \tag{25}$$

3.6.4 Porosity evolution

As the elimination of SiC during the oxidation increases the porosity, whereas the formation of silica SiO_2 clogs gradually the voids, the change in the porosity ϕ (Eq. 14) from the initial state ϕ_0 resulting only from the oxidation process (Eq. 1) is defined as

$$\phi = \phi_0 - \left(\frac{M_{SiO_2}}{\rho_{SiO_2}} - \frac{M_{SiC}}{\rho_{SiC}} \right) \xi \tag{26}$$

where ρ_{SiO_2} and ρ_{SiC} are the mass density of dense SiO and SiC respectively and M_{SiO_2} and M_{SiC} are the molar mass of SiO and SiC respectively.

3.7 Identification of oxidation kinetics

The link between the mass change and the chemical extent is used to identify the kinetics of oxidation. When a sample having a initial mass m_0 and an initial volume V_0 is subjected to an oxidation process, its mass change, Δm, can be estimated by integrating the local mass balance (Eq. 3) over the volume $V \approx V_0$

$$\frac{\Delta m}{m_0} = \frac{1}{m_0} \int_{V_0} \left(\left(M_{SiO_2} \nu_{SiO_2} + M_{SiC} \nu_{SiC} \right) \xi \right) dV \tag{27}$$

In Eq. 27 only the solid phases are accounted for because the gaseous phase trapped in the porosity and disappearing during the oxidation has no effect on the weight of the sample. For large samples, as a gradient of ξ exists in the bulk a chemio-diffusion simulation of the samples by finite element method must be performed for an accurate identification of the parameters of the kinetics law. Δm is then calculated as follows

$$\frac{\Delta m}{m_0} = \frac{M_{SiO_2} - M_{SiC}}{m_0} \sum_{i}^{N_{FE}} \xi^i V^i \tag{28}$$

where V^i is the volume of each finite element i and ξ^i the associated chemical extent density calculated at the integration points and N_{FE} the number of finite elements.

The identification of the oxidation kinetics of SiC-RC was done thanks experimental results from the isothermal TGA detailled previously (Fig. 2a). Two reasonable assumptions were made to achieve the identification: diffusion of gases inside the samples are very fast and oxidation is homogeneous, as the samples were small -the initial mass was less than 2g- and the porosity was not clogged at the end of the test.

Equation 28 of the mass change was used to identify the oxidation kinetic parameters: k_p^0 and E_p (Eq. 19). First, the rate constant k_p was identified from the experimental curve for each temperature. Then the activation energy E_p and the pre-exponential factor k_p^0 were deduced. The obtained values are $k_p^0 = 2.4 \times 10^{-11}$ s^{-1} and $E_p = 187.35$ kJ·mol^{-1}. Depending on the sample conditions (bulk, film or powder, single crystal or poly-crystals) and testing environments, E_p is ranged from 100 kJ·mol^{-1} to 500 kJ·mol [6,13,14,20]. For example, E_p of the oxidation of SiC powder is 213.1 kJ/mol [6]. For the chemical vapour deposition (CVD) SiC pellet it is equal to 118.1 kJ·mol^{-1} [5,15]. So, E_p is in the middle range of literature's values. As the proposed definition of k_p^0 is quite original, no estimate from literature is available right now. Comparison between the model and experimental results are presented on Fig. 6.

3.8 Identification of the chemical swelling

The identification of the parameters β and ξ_{cr} of the chemical induced strain (Eq. 23) requires to correlate the strain to the oxidation extent. Assuming a homogeneous oxidation in the small sized samples during isothermal dilatometry tests, after the same duration, the oxidation extent is assumed being the same than that in a TGA sample. This assumption is reasonable in this study but for a very long duration, the clog of the porosity may invalidate the homogeneity assumption. Consequently the experimental result can not be identified by the previous simplified procedure but with numerical simulations using finite element method.

The isothermal dilatometry tests were combined with the ATG test for the identification of chemical strain. From Fig. 7a and using the equation of mass change (Eq. 28), the evolution of oxidation extent ξ was deduced. The curve ξ versus $\dfrac{\Delta L}{L}$ is then plotted in Fig. 7. This figure shows also at the abscissa the oxidized SiC proportion.

It is remarkable that, beyond a critical value of the oxidation extent, there is a linear relationship between the chemical expansion and the oxidation extent in accordance with the adopted assumption (Eq. 23). The discrepancy in the experimental and theoretical curves observed at the beginning may correspond to the shrinkage induced by the last stage of sintering of the matrix binder. It is not taken into account in the present modelling. This effect is encompassed in the definition (23) of the critical extent. Finally, the slope of the linear dependence between chemical strain and extent has been identified equal to 2.647×10^{-3} $\mathrm{m}^3{\cdot}\mathrm{kmol}^{-1}$.

4 Finite element modelling of an oxidation test under thermal gradient

The numerical simulations were made with the FE code Abaqus® [40]. To solve the set of constitutive and balance equations developed in the previous sections, which are partially uncoupled, the computations performed in three successive steps:

- the heat transfer equations are solved in the first step,
- the reactive transport of gas through the porosity under thermal gradient equations are solved in the second step,
- the mechanical problem, accounting for mechanical behaviour (homogeneous isotropic elasticity), temperature field and oxidation extent field (inducing chemical expansion) is solved in the third step.

To perform the reactive transport computation, the mass balance (Eq. 24) was implemented in the finite element code via the User MATerial Heat Transfer subroutine UMATHT [40]. For the mechanical step, the thermal and chemical strains were implemented thanks to the User EXPANsion subroutine UEXPAN which allows to define incremental strains combined with mechanical behaviour library [40].

In order to validate the model developed previously, a numerical simulation was done of the experimental oxidation test of the cylindrical sample subjected to thermal gradient for a duration of 56 days (see. section 2.3). Axisymmetrical model was considered for the finite element analysis (Fig. 3).

Perfect thermal contact between the castable and the insulator was applied. Radiative heating flux was applied between the oven and the insulator, the heating resistors and the concrete, the concrete and the oven (1150 ^{o}C) with an emissivity of $\epsilon = 0.9$. Temperature level of $T_h = 1150$ ^{o}C was considered on the heating resistors. Pn the bottom of the concrete specimen thermal convection with the ambient (20 ^{o}C) with a heat transfer coefficient $h = 25$ W.K^{-1}.m^{-2} was applied. An oxygen partial pressure equal to $P_{O_2} = 0.21$ atm (i.e. air) was imposed at the boundaries of the specimen. The activation temperature of SiC oxidation was fixed to 850 ^{o}C.

To ensure a realistic mechanical equilibrium, axial displacement of the bottom face was prevented. The oven was not taken into account for the mechanical computation as there was no contact between the sample and the oven. As the fibrous insulation wrapping the sample was flexible, it was not taken into account for the mechanical computation too.

The finite element model and boundary conditions are shown in Fig. 3. The material properties for the SiC based castable used for the simulation were those previously identified as well as data extracted from the literature. Thermal properties of the insulator are reported in Table 1 which gathers all the material properties used in the computation.

Figure 8a shows the stationary temperatures along the axis of the cylinder obtained by simulation and experiment. The results are in good agreement, the temperature of the thermocouples being well reproduced by the model. It validates the thermal boundary conditions and the assumptions made for the energy balance. The stationary temperature field is reached after several hours, so the transient period can be neglected to compute the reactive transport. For

this computing step, a temperature stationary state for all the 56 days duration of the test was applied to reduce the computation cost. Then, the oxidation extent field at the end of the computation was used in the thermomechanical simulation to compute the chemical strain.

Figure 9 shows the variation in diameter all along the cylinder predicted by the numerical simulation and the experimental results after 56 days. The model gives an appropriate description of physical phenomena since a rather good agreement between the experimental and numerical results can be observed. The combined effect of thermal gradient and of oxidation induces a higher swelling at the hot face. It is firstly due to the thermal activation of oxidation and, secondary, it is linked to the slow down of the oxygen transport induced by the matrix densification.

5 Discussions

The thermo-chemo-mechanical model predicts a final swelling after 56 days close to the experimental residual strain characterised by the diameter variation profile, as shown on Fig. 8b. The discrepancy is lower than 20% for a distance from the hot face lower than 40 mm. In the 40 to 80 mm range, the macroscopic strain is smaller and the difference too.

To check the porosity evolution, SEM micrograph pictures and model predictions are compared (Fig. 10). Observations of the microstructure show that the silicon carbide grains in the matrix are oxidized. In the upper zone of the sample, where temperature is high enough and where diffusion of oxygen in the porosity occurs, grains in the matrix are covered with a silica layer.

Due to this silica layer a densification of the matrix is observed. This phenomenon is observed at the hot face and at distances from the hot face lower than 40 mm. For distances greater than 40 mm, no silica layer was observed with SEM as the oxidation of the SiC was too low. These observations are in good accordance with the assumption concerning the porosity clog up by the silica produced by the SiC oxidation. Moreover, the porosity evolution with depth predicted by the computation is in qualitative agreement with the SEM observation.

To illustrate the impact of the porosity clog up for long oxidation durations, the evolution of the ratio of the effective diffusion coefficient $D_e =$ to the diffusion coefficient in free paths D_a is drawn up in Fig. 11. The evolution of this ratio with time considering the hot face of the specimen (Fig. 11a) underlines that the effect becomes visible after more than 50 days. That corresponds to a relative radius reduction of the smaller pores of more than 0.5, that to say a radius reduction of more than 50%.

Figure 12 presents the result of FE simulation considering a two-year oxidation duration under thermal gradient. A great difference between computations accounting or not for porosity clog up is noticed. Indeed, neglecting this effect leads to a large overestimation of the tile's oxidation and of the global swelling. The numerical simulation exhibits the formation of a small layer of totally closed porosity on the hot face which protects the tile. In our test, oxygen still arrives through lateral face, but it will not be the case for large castable panels in service. This phenomenon may explain the large lifespan in service, compared to simplified predictions of SiC based refractory oxidation realized on the extrapolation of results obtained on SiC grains or powders.

6 Conclusion

A multiphysic model has been developed to describe swelling effects due to the oxidation of SiC-based refractory castable. This model has been built in the framework of the thermodynamics of irreversible processes for reactive porous multi-phase materials. Reasonable assumptions have been made to partially uncouple some physical phenomena allowing to made numerical simulations in the finite element code Abaqus® thanks to some tricks and the implementation of some equations in user subroutines. Consequently, simulations can be carried out in three successive steps, namely heat transfer, reactive transport under thermal gradient and the thermomechanics accounting for swelling induced by the oxidation.

A simplified model of oxidation kinetics and associated chemical strain has been used. Many many parameters have been taken from literature or estimated. Its ability to predict the shape of a cylinder of SiC-based castable under high temperature gradient for a long oxidation time has been demonstrated.

The proposed thermo-chemo-mechanical model gives an appropriate description of physical phenomena since a rather good agreement is obtained with SEM observations and macroscopic measurements. Such results allow to validate the ability of the model to predict fairly well the swelling induced by the oxidation of part made of a SiC-based refractory castable. The quantitative error on the shape variation is reasonable in regard to refractory applications. Nevertheless, experimental developments have to be performed to increase the accuracy of the model prediction by accurate identification of all parameters.

¿From a general point of view, this work constitutes one more step to reinforce the methodology to study and model thermo-chemo-mechanical couplings in the field of refractories. It is noteworthy that there is no difficulty to introduce more complex chemical reactions that induce chemical swelling in this model based on strain partition and classical thermochemistry. However, it should be kept in mind the necessity to reduce the physical parameters to be identified because of the difficulty to access to reliable data at high temperatures.

Acknowledgements

The authors wish to thank French Research National Agency (ANR) for granted the DRuiDe program, and all partners for fruitful discussions and experimental tests.

References

[1] W. Lee, R. Moore, Evolution of in situ refractories in the 20^{th} century, Journal of the American Ceramic Society 81 (6) (1998) 1385–1410.

[2] J. Poirier, Ceramic Materials: Processes, Properties and Applications. Chapter 10 Refractory materials, IDTE Ltd, 2007.

[3] E. Blond, N. Schmitt, F. Hild, P. Blumenfeld, J. Poirier, Effect of slag impregnation on thermal degradations in refractories, Journal of the American Ceramic Society 90 (1) (2007) 154–162.

[4] N. Schmitt, Y. Berthaud, J. Hernandez, P. Meunier, J. Poirier, Damage of monolithic refractory linings in steel ladles during drying, British Ceramic Transactions 103 (3) (2004) 121–133.

[5] X. Hou, K. Chou, F. Li, A new treatment for kinetics of oxidation of silicon carbide, Ceramics International 35 (2) (2009) 603–607.

[6] Y. Lin, L. Chen, Oxidation of SiC powders in SiC/alumina/zirconia compacts, Ceramics International 26 (6) (2000) 593–598.

[7] P. Prigent, M. L. Bouchetou, J. Poirier, Corrosion of sic based refractories by molten salts in municipal solid waste to energy facilities, 49th conference on metallurgists, COM 2010, Vancouver.

[8] P. Prigent, Approche multi-échelle des mécanismes de corrosion *à* haute température des céramiques réfractaires : Application *à* la dégradation de carbures de silicium par les sels, Ph.D. thesis, University of Orléans, France (2010).

[9] P. Prigent, E. de Bilbao, N. Schmitt, J. Poirier, E. Blond, M. L. Bouchetou, Measurement of the volume expansion of SiC refractories induced by molten

salts corrosion, Proceeding of Unitecr 2011, Kyoto, CDRom and abstract 1-E-3 p.70.

[10] C. Zheng, Z. Yang, J. Zhang, The high-temperature oxidation behavior of reaction-bonded porous silicon carbide ceramics in dry oxygen, Journal of the American Ceramic Society 93 (7) (2010) 2062–2067.

[11] A. Gallet-Doncieux, O. Bahloul, C. Gault, M. Huger, T. Chotard, Investigations of SiC aggregates oxidation: Influence on SiC castables refractories life time at high temperature, Journal of the European Ceramic Society 32 (4) (2012) 737 – 743.

[12] Y. Li, Y. Yang, Z. Lin, J. Li, Investigation of isothermal and no-isothermal oxidation of SiC powder using an analytic kinetic model, Applied Surface Science 257 (2) (2010) 463–467.

[13] W. Pultz, Temperature and oxygen pressure dependence of silicon carbide oxidation, Journal of Physical Chemistry 71 (13) (1967) 4556–4558.

[14] D. Liu, Oxidation of polycrystalline α-silicon carbide ceramic, Ceramics International 23 (5) (1997) 425–436.

[15] L. Ogbuji, E. Opila, A comparison of the oxidation kinetics of SiC and Si_3N_4, Journal of The Electrochemical Society 142 (1995) 925–930.

[16] D. Das, J. Farjas, P. Roura, Passive-oxidation kinetics of SiC microparticles, Journal of the American Ceramic Society 87 (7) (2004) 1301–1305.

[17] J. Eck, M. Balat-Pichelin, L. Charpentier, E. Bêche, F. Audubert, Behavior of SiC at high temperature under helium with low oxygen partial pressure, Journal of the European Ceramic Society 28 (15) (2008) 2995 – 3004.

[18] B. Schneider, A. Guette, R. Naslain, M. Cataldi, A. Costecalde, A theoretical and experimental approach to the active-to-passive transition in the oxidation

of silicon carbide: Experiments at high temperatures and low total pressures, Journal of Materials Science 33 (1998) 535–547.

[19] J. Wang, L. Zhang, Q. Zeng, G. L. Vignoles, L. Cheng, A. Guette, The rate-limiting step in the thermal oxidation of silicon carbide, Scripta Materialia 62 (9) (2010) 654657. doi:10.1016/j.scriptamat.2010.01.017.

[20] S. C. Singhal, Oxidation kinetics of hot-pressed silicon carbide, Journal of Materials Science 11 (1976) 1246–1253.

[21] J. Antill, J. Warburton, Active to passive transition in the oxidation of SiC, Corrosion Science 11 (6) (1971) 337 – 342.

[22] T. Goto, H. Homma, High-temperature active/passive oxidation and bubble formation of CVD SiC in O_2 and CO_2 atmospheres, Journal of the European Ceramic Society 22 (14-15) (2002) 2749 – 2756.

[23] O. Bahloul, Evolutions en fonction de la température de propriétés élastiques de bétons réfractaires à base de carbure de silicium, Ph.D. thesis, University of Limoges, France (2009).

[24] F.-J. Ulm, E. Lemarchand, F. H. Heukamp, Elements of chemomechanics of calcium leaching of cement-based materials at different scales, Engineering Fracture Mechanics 70 (2003) 871889.

[25] D. Kuhl, F. Bangert, G. Meschke, Coupled chemo-mechanical deterioration of cementitious materials. part i: Modeling, International Journal of Solids and Structures 41 (2004) 1540.

[26] V. Nguyen, B. Nedjar, J. Torrenti, Chemo-mechanical coupling behaviour of leached concrete: Part ii: Modelling, Nuclear Engineering and Design 237 (2007) 20–21.

[27] C. Comi, R. Fedele, U. Perego, A chemo-thermo-damage model for the analysis

of concrete dams affected by alkali-silica reaction, Mechanics of Materials 41 (2009) 210–230.

[28] D. Gawin, F. Pesavento, B. Schrefler, Modelling of hygro-thermal behaviour of concrete at high temperature with thermo-chemical and mechanical material degradation, Computer Methods in Applied Mechanics and Engineering 192 (13-14) (2003) 1731–1771.

[29] O. Coussy, Deformation and stress from in-pore drying-induced crystallization of salt, J. Mech. Phys. Solids 54 (2006) 15171547.

[30] O. Coussy, Mechanics and physics of porous solids, Wiley & Sons, 2010.

[31] H. Callen, Thermodynamics, Wiley, 1960.

[32] R. B. Bird, W. E. Stewart, E. N. Lightfoot, Transport phenomena (Second Edition), Wiley & Sons, 2002.

[33] W. Yiguang, S. Yongho, A. Linan, F. Yi, Z. Ligong, Oxygen diffusion through Al-doped amorphous SiO_2, Journal of Phase Equilibria and Diffusion 27 (2006) 671–675.

[34] A. Atkinson, A. K. Nickerson, The diffusion of ions through water-saturated cement, Journal of Materials Science 19 (1984) 3068–3078.

[35] P. Grathwohl, Diffusion in natural porous media: Contaminant transport, sorption/desorption and dissolution kinetics, Kluwer Academic Publishers, 1998.

[36] L. Shen, Z. Chen, Critical review of the impact of tortuosity on diffusion, Chemical Engineering Science 62 (14) (2007) 3748–3755.

[37] I. Prigogine, Introduction to thermodynamics of irreversible processes, Interscience Publishers, 1967.

[38] A. Haxaire, I. Djeran-Maigre, Influence of dissolution on the mechanical behaviour of saturated deep argillaceous rocks, Engineering Geology journal 109 (2009) 255–261.

[39] V. Presser, A. Loges, Y. Hemberger, K. G. Nickel, Microstructural evolution of silica on single-crystal silicon carbide. part 1: Devitrification and oxidation rates, Journal of the American Ceramic Society 92(3) (2009) 724–731.

[40] Abaqus Manual 6.10 EF, 2011.

[41] Ceramic fiber paper, Nutec Fibratec.

[42] O. Bahloul, T. Chotard, M. Huger, C. Gault, Young's modulus evolution at high temperature of SiC refractory castables, Journal of Materials Science 45 (2010) 3652–3660.

[43] Calderys data, Calderys Refractory Solutions.

Insulator fiber [41]	Thermal conductivity λ_f $(W/m/K)$	0.054 (204^oC)
		0.279 (1093^oC)
	Specific heat c_f $(J/kg/K)$	1000
	Mass density ρ_f (kg/m^3)	185
SiC based castable	Young's modulus E (GPa) [42]	110
	Poisson's ratio ν [42]	0.2
	Coefficient of thermal expansion α $(1/K)$ [43]	5.10^{-6}
	Thermal conductivity λ $(W/m/K)$ [43]	7.6 (20-800^{o}C)
		8.8 (1000^{o}C)
	Specific heat c $((J/kg/K))$ [43]	1130
	Mass density ρ (kg/m^3) [43]	2500
	Initial porosity ϕ_0 (%) [43]	16
	Coefficient of chemical strain β $(m^3/kmol)$	2647×10^{-6}
	Pre-exponential rate constant k_p^0 $(1/s)$	2.4×10^{-11}
	Activation energy of oxidation E_p (kJ/mol)	187.35
	Molar mass of SiO_2 M_{SiO_2} (g/mol)	60
	Molar mass of SiC M_{SiC} (g/mol)	40
	Mass density of SiO_2 ρ_{Si0_2} (kg/m^3)	2100
	Mass density of SiC ρ_{SiC} (kg/m^3)	3220

Table 1

Data used for the FE simulation of the oxidation test under thermal gradient

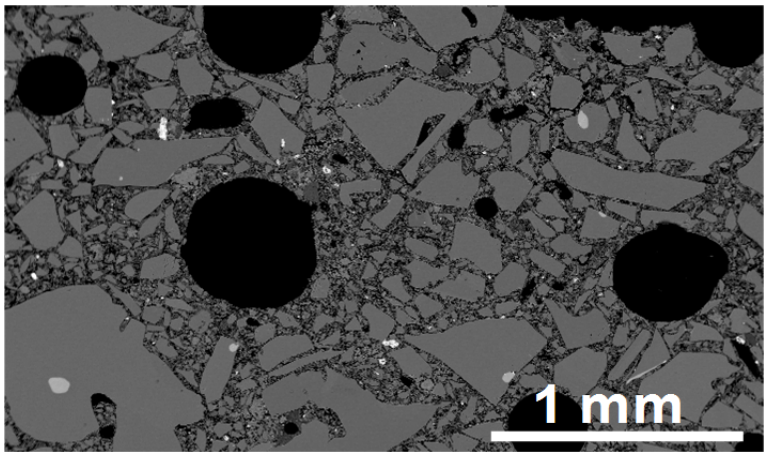

(a) Castable (grains and matrix)

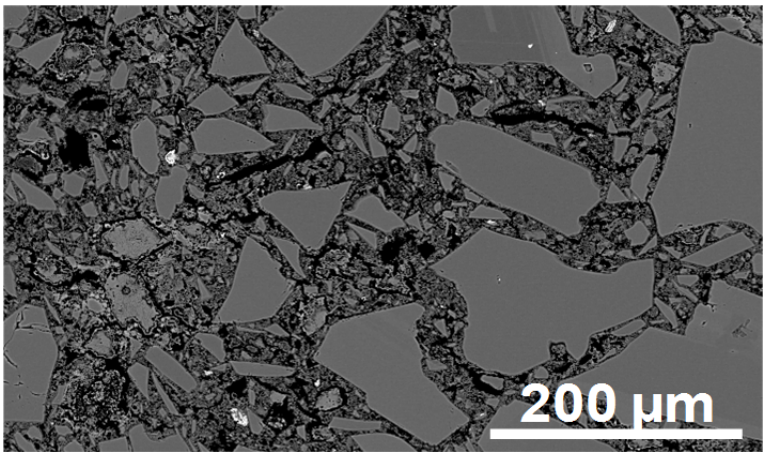

(b) Detail of the matrix

Figure 1. SEM backscattered electron micrographs on a polished cross section of SiC-RC

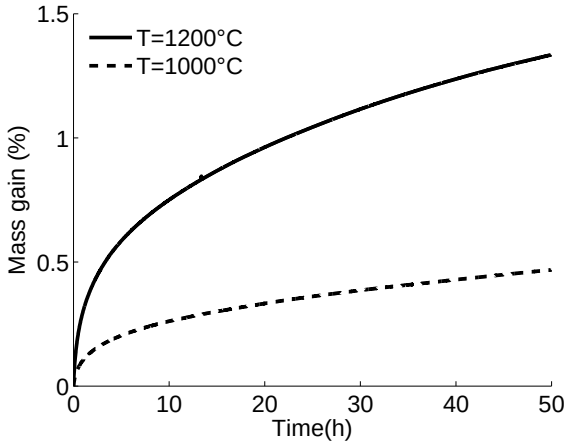

(a) Mass gain

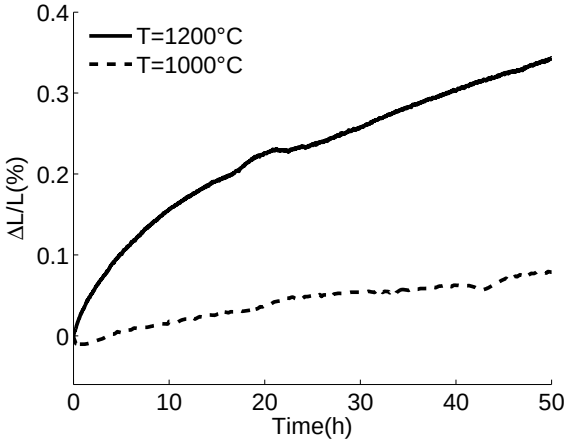

(b) Isothermal dilatometry

Figure 2. Mass gain and chemical induced expansion versus time at 1000 ^oC and at 1200 ^oC

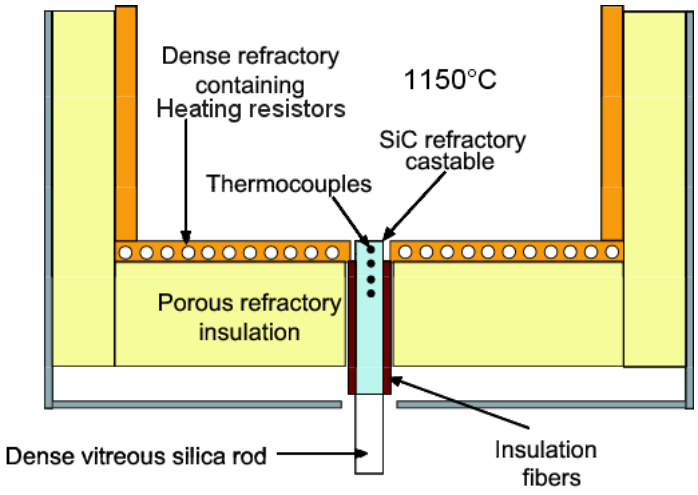

Figure 3. Experimental set-up for the oxidation test under thermal gradient

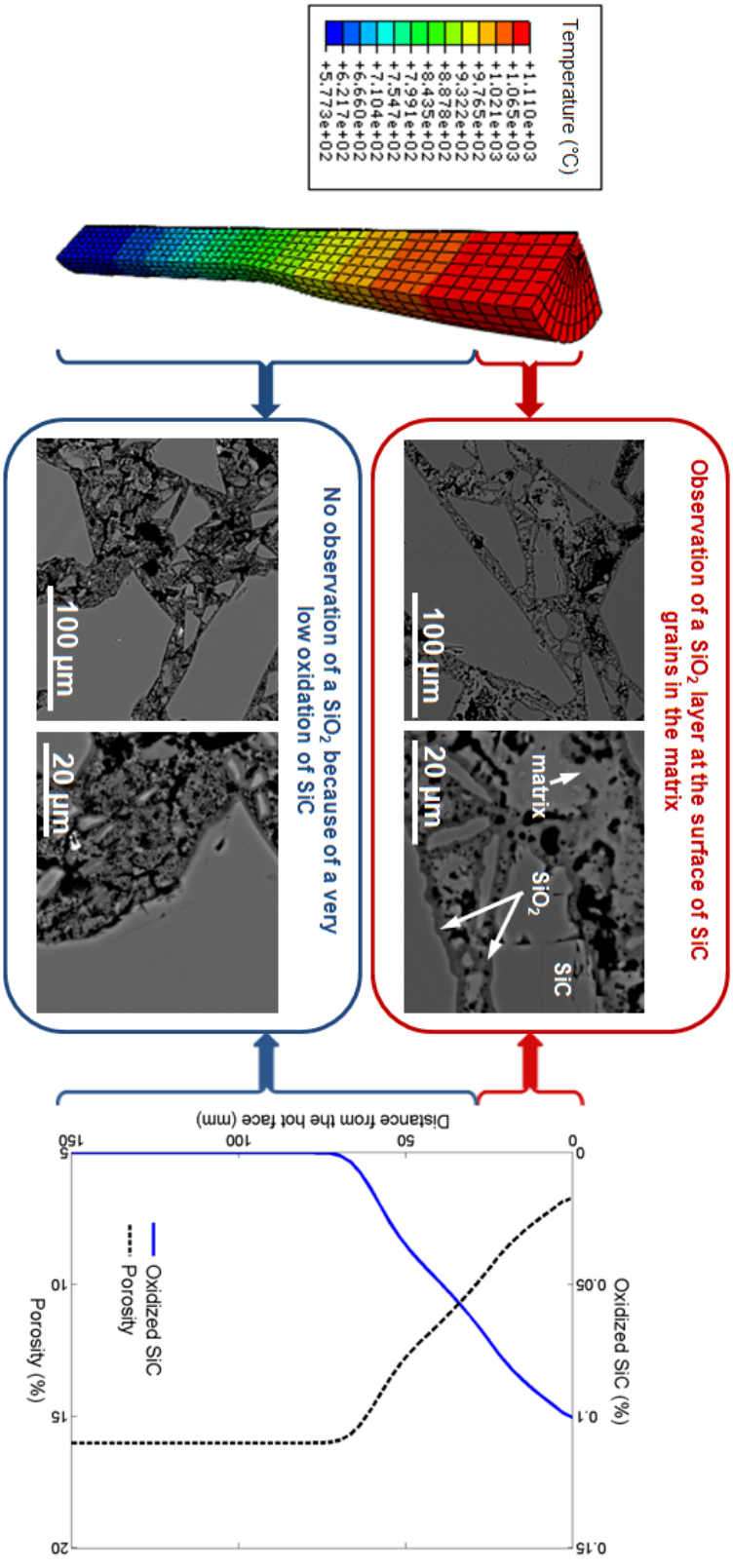

Figure 10. Comparison of the results of finite element simulation for 56 days of oxidation and SEM observations on the oxidized sample

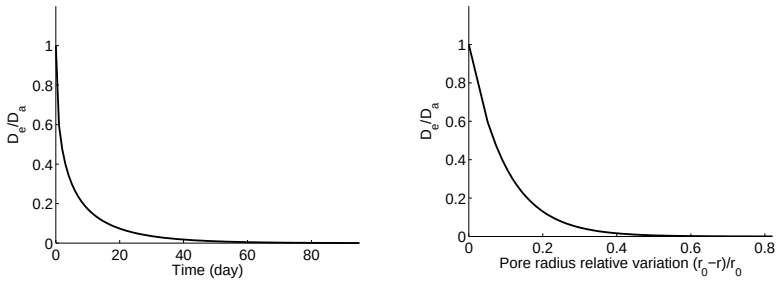

(a) (b)

Figure 11. Evolution of the effective diffusion / diffusion coefficient in free space

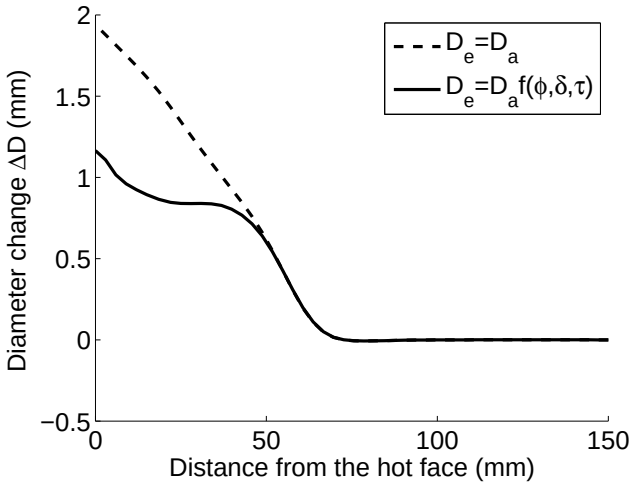

Figure 12. Results of finite element simulation of the diameter change versus the distance from the hot face after a 2 years long oxidation test

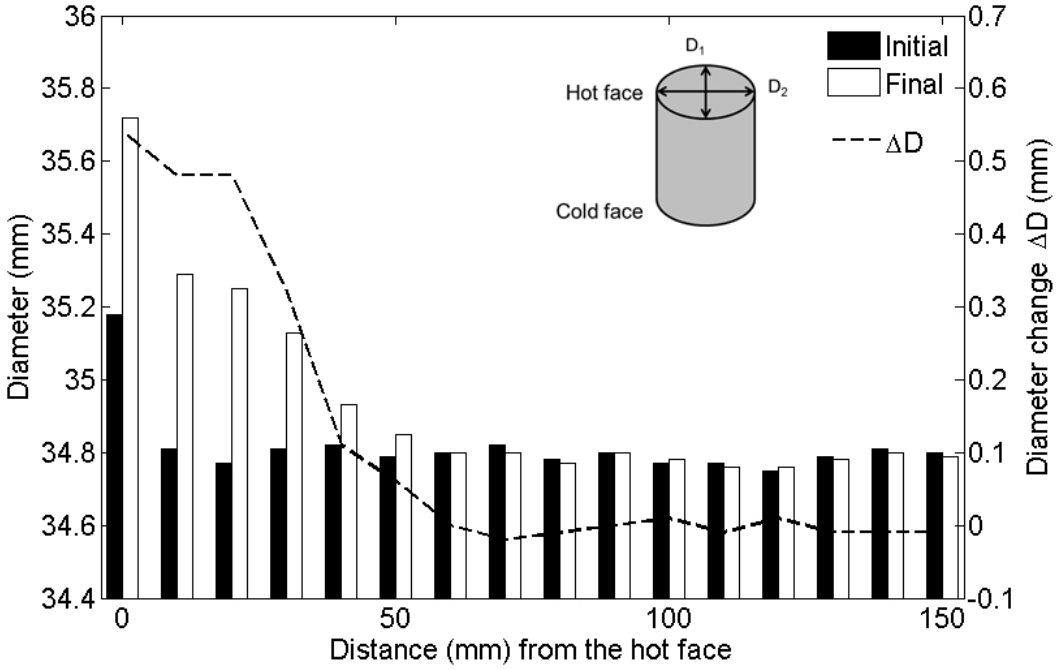

(a) D_1

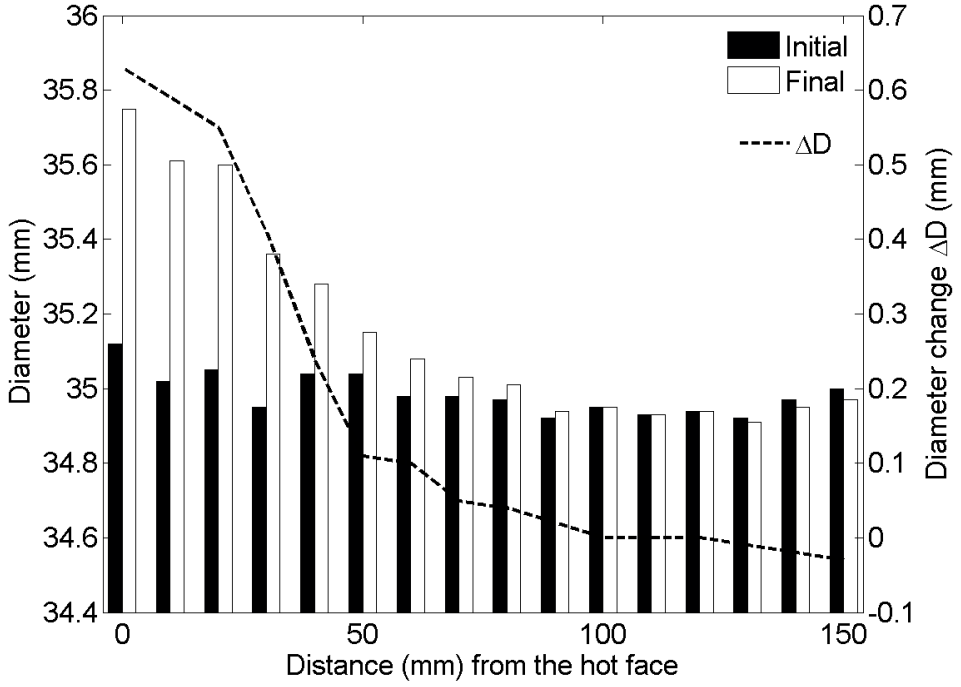

(b) D_2

Figure 4. Evolution of the two orthogonal diameters of the sample versus the distance from the hot face

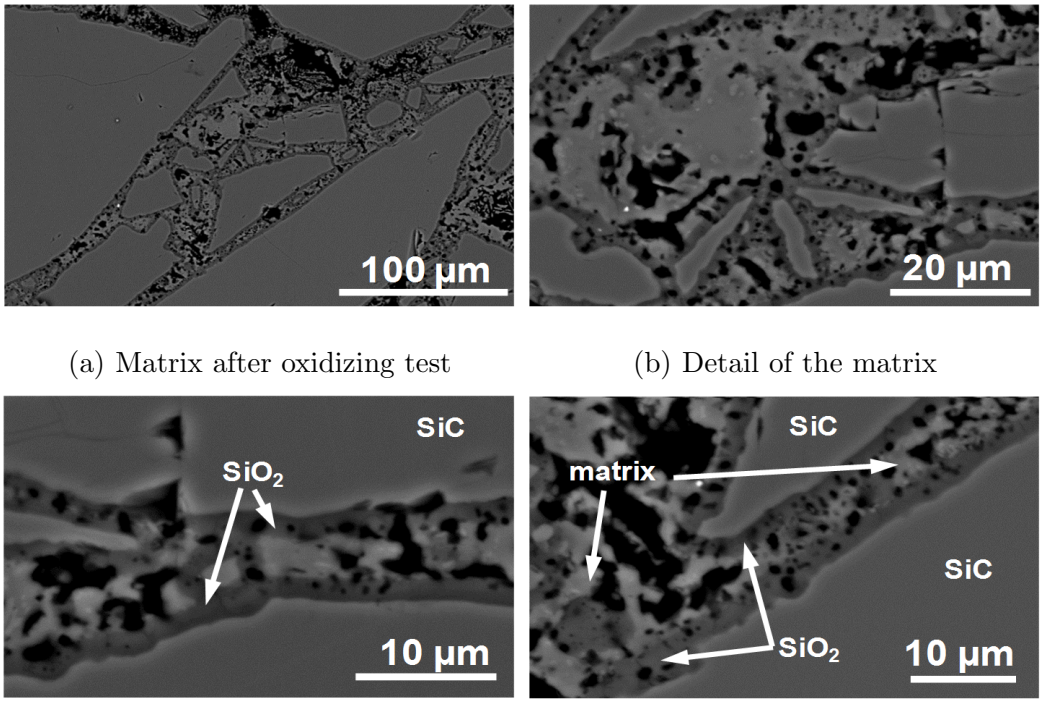

(a) Matrix after oxidizing test (b) Detail of the matrix

(c) Detail of the matrix (d) Detail of the matrix

Figure 5. SEM backscattered electrons micrographs on a polished cross section of the considered refractory castable (at a distance of 5 mm from the hot face) after the oxidizing test

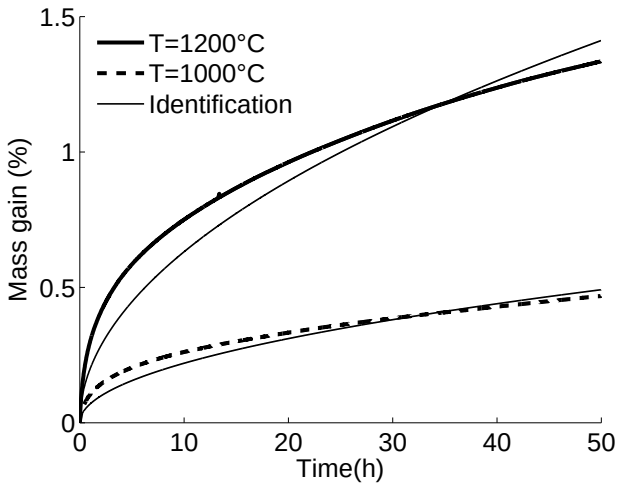

Figure 6. Mass gain predictions and experimental measurements

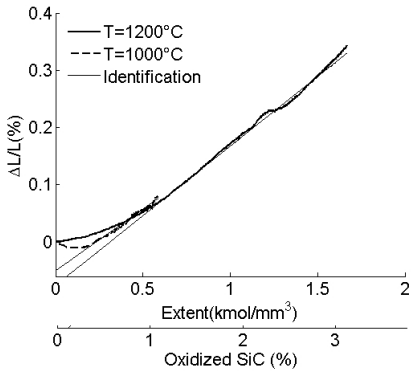

Figure 7. Chemical induced expansion versus oxidation extent (or oxidized SiC proportion) for two temperatures

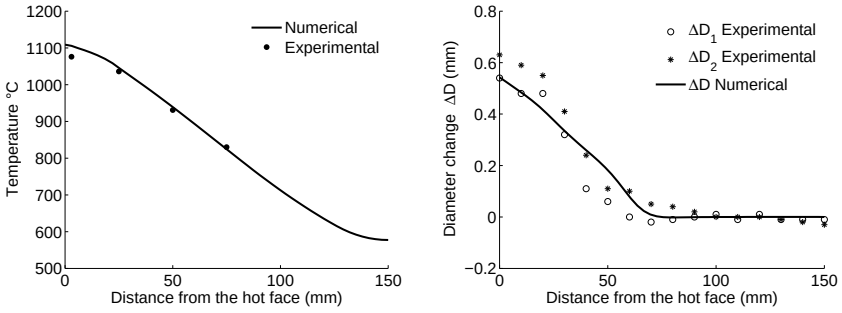

(a) Temperature field (b) Diameter variation

Figure 8. Numerical results for a 56 days oxidation duration

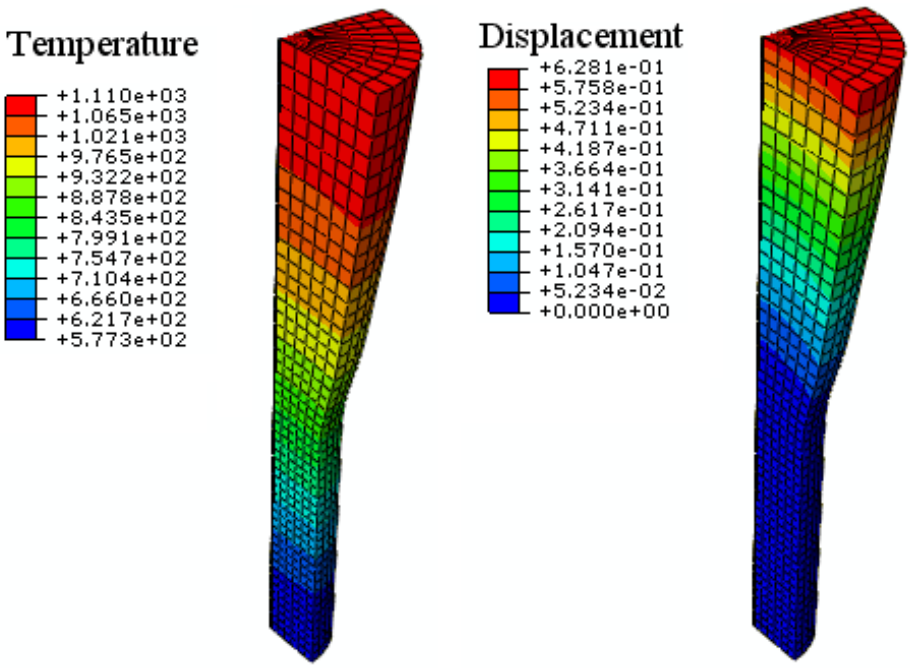

(a) (b)

Figure 9. Results of finite element simulation for 56 days of oxidation: a) Thermal field (^oC), b) Displacement (mm) (amplification factor 50)